Substitutional disorder and optical spectroscopy of Ce^{3+}-doped $CaNaYF_6$ crystals

2001 J. Phys.: Condens. Matter 13 753

(http://iopscience.iop.org/0953-8984/13/4/321)

INSTITUTE OF PHYSICS PUBLISHING JOURNAL OF PHYSICS: CONDENSED MATTER

J. Phys.: Condens. Matter **13** (2001) 753–764 www.iop.org/Journals/cm PII: S0953-8984(01)14983-0

Substitutional disorder and optical spectroscopy of Ce^{3+}-doped $CaNaYF_6$ crystals

M Yamaga[1], T Imai[1], H Miyairi[1] and N Kodama[2]

[1] Department of Electrical and Electronic Engineering, Faculty of Engineering, Gifu University, Gifu, 501-1193, Japan
[2] Department of Materials Science and Engineering, Faculty of Engineering and Resource Science, Akita University, Akita, 010-8502, Japan

Received 21 June 2000, in final form 28 November 2000

Abstract

$CaNaYF_6$ (CNYF) single crystals doped with Ce^{3+} have the CaF_2-type cubic-fluorite structure where Ca^{2+}, Na^+, and Y^{3+} randomly occupy the common cation sites. The optical absorption and luminescence spectra of Ce^{3+} in the CNYF crystal, being broadened by a strong electron–phonon interaction in the 5d excited state, have a large Stokes shift. Substitutional disorder in the CNYF crystal produces inhomogeneous broadening of the optical spectra and a distribution of the lifetime of the Ce^{3+} luminescence. The linewidth and lifetime are discussed in terms of a distribution of the crystal-field splitting of the 5d excited state of Ce^{3+} in the CNYF crystal.

1. Introduction

There is much interest in Ce^{3+}-doped ionic crystals for applications in scintillators and tunable lasers [1, 2]. Ce^{3+} ions are represented by a simple one-electron system. The electron configurations of the ground and excited states of Ce^{3+} are $4f^1$ and $5d^1$, respectively. The ^2F_J ground state of $4f^1$ is split by spin–orbit interaction into the $^2F_{5/2}$ and $^2F_{7/2}$ levels separated by $\sim$2200 cm^{-1}. On the other hand, the ^2D_J excited state of $5d^1$ is affected much more strongly by crystal-field interaction than is ^2F_J. If the crystal-field interaction for $5d^1$ is much larger than the spin–orbit interaction, then the ^2D_J excited state is split into five Kramers doublets by low symmetry.

Optical absorption in Ce^{3+}-doped crystals corresponds to the transitions from the $^2F_{5/2}$ ground state to the five $5d^1$ excited states, whereas luminescence occurs as the transitions from the lowest $5d^1$ excited state to the $^2F_{5/2}$ and $^2F_{7/2}$ ground states. A large electron–phonon coupling for the $5d^1$ state produces a large Stokes-shift energy $2S\hbar\omega$ (S: Huang–Rhys factor; $\hbar\omega$: phonon energy) between the absorption and luminescence spectra [3]. In consequence, the absorption spectrum consists, at most, of five overlapping broad bands, while the luminescence spectrum has two broad bands with the energy separation of $\sim$2200 cm^{-1}. The optical absorption and luminescence spectra in the UV region observed for the Ce^{3+}-doped fluoride crystals $LiYF_4$ (LYF) [4, 5] and $LiCaAlF_6$ (LiCAF) [6, 7] are due to Ce^{3+} substituting

0953-8984/01/040753+12$30.00

at ordinary sites with S_4 and C_{3v} symmetry, respectively, in these crystals. In a previous paper [8], a brief report of the results for the optical spectra of Ce^{3+} in $CaNaYF_6$ (CNYF) crystals with the CaF_2-type cubic-fluorite structure, where Ca^{2+}, Na^+, and Y^{3+} ions randomly occupy the common cation sites, has been given.

This paper describes the effects of substitutional disorder in the CNYF crystal on the inhomogeneous broadening of the Ce^{3+} luminescence and a distribution of the lifetime. We discuss the optical data in terms of a distribution of the crystal-field splitting of the $5d^1$ excited state of Ce^{3+} in the CNYF crystal in comparison with those observed for various Ce^{3+}-doped fluoride and oxide crystals.

2. Crystal structure and experimental procedure

The $CaNaYF_6$ (CNYF) crystal has the CaF_2-type cubic-fluorite structure with space group O_h^5, where Ca^{2+} is eightfold coordinated. The ions Ca^{2+}, Na^+, and Y^{3+} randomly occupy their common cation-lattice sites, cube corners (0, 0, 0), and face-centred positions in the unit cell. The composition ratio of Ca^{2+}, Na^+, and Y^{3+} is maintained at 1:1:1. Each metal ion forms a cube composed of eight F^- ligand ions. The cubes are modified by a random distribution of Ca^{2+}, Na^+, and Y^{3+} located at the second-nearest-neighbour and further-neighbour cation sites. The variation of the crystal fields of these cubes may be not discrete but continuous; that is, the cubes with central ions Ca^{2+}, Na^+, and Y^{3+} may be not distinguished as different unique environments in the crystal. However, the environments are expected to be classified into ordered and disordered configurations of the second-nearest-neighbour cations [9, 10].

Ce^{3+} ions substitute for Ca^{2+}, Na^+, and Y^{3+} ions occupying their common cation sites. We cannot say which ion Ce^{3+} substitutes for, because the charge balance in the crystal is satisfied through a distribution of Ca^{2+}, Na^+, and Y^{3+} ions at the near cation sites or through interstitial F^--ion compensators [11]. It seems that Ce^{3+} ions preferentially substitute for Y^{3+} ions within various configurations in the CNYF crystal because the trivalent rare-earth ions require similar environments.

The Ce^{3+}-doped CNYF single crystals were grown in a reducing atmosphere by spontaneous crystallization from slowly cooled melts. The starting charge was formed from a stoichiometric mixture of CaF_2, NaF, and YF_3 with a mol.% ratio of 1:1:1. The concentration of CeF_3 relative to that of YF_3 was 4 mol.%, resulting in 4/3 at.% Ce^{3+} concentration relative to that of the cations. Crystal boules of dimension 20 mm diameter by 5 mm length were obtained. The bulk crystals were optically transparent and free of entrapped inclusions. The lattice constant was obtained as $a = 5.535$ Å by means of x-ray diffraction.

Optical absorption spectra were measured using a Hitachi U-3500 spectrophotometer at 300 K in the range of 190–2500 nm. Luminescence and excitation spectra were also measured at 300 K using a Hitachi F-4500 fluorescence spectrophotometer. The lifetime of the luminescence was measured using a Horiba NAES-700F time-resolved photoluminescence spectrometer at 77 and 300 K in the Instrumental Analysis Centre, Gifu University.

3. Experimental results

Figure 1 shows the optical absorption spectrum of Ce^{3+} in the CNYF crystal. The spectrum consists of four intense bands with peaks at 211, 258, 297, and 312 nm in the range of 190–400 nm. UV excitation, for example, at 300 nm, produces an intense luminescence band with a peak at 360 nm denoted by A_1 with a tail to long wavelengths denoted by A_2 as shown in figure 2(a). The peak of the A_1 band is constant in the excitation range of 200–310 nm

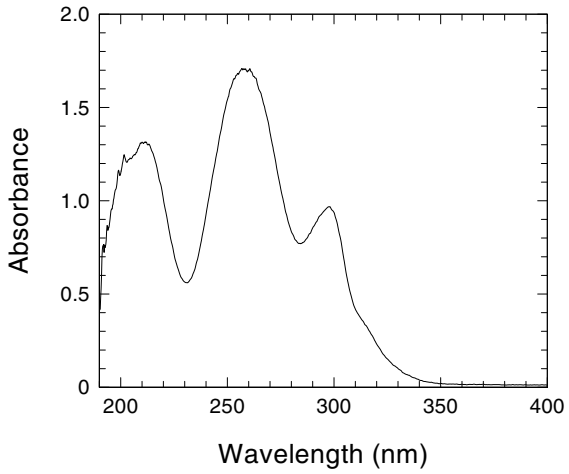

Figure 1. The absorption spectrum of Ce^{3+} in $CaNaYF_6$ measured at 300 K.

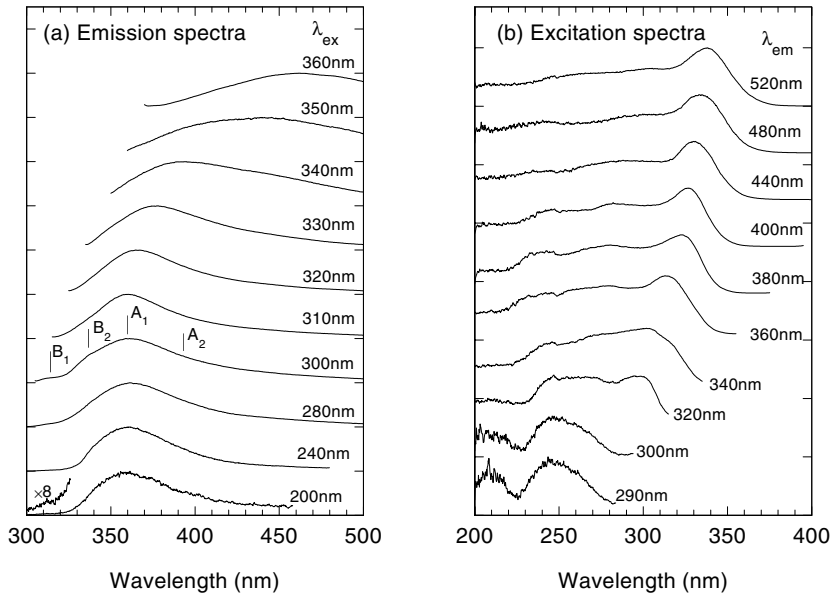

Figure 2. (a) The luminescence spectra of Ce^{3+} in $CaNaYF_6$ excited with different wavelengths measured at 300 K. The (A_1, A_2) and (B_1, B_2) bands denote different luminescent centres. (b) The excitation spectra obtained by monitoring the intensities of the Ce^{3+} luminescence at different fixed wavelengths in $CaNaYF_6$ measured at 300 K.

and shifted gradually to longer wavelengths when the excitation wavelength increases above 310 nm. The luminescence spectrum excited at 340 nm consists of two overlapping bands with nearly equal intensities. The luminescence spectrum excited at 350 nm becomes a fairly broad band with a large peak shift. The large width is explained by the fact that the A_2 band competes in intensity with the A_1 band. In addition, excitation below 300 nm produces two weak bands with peaks at 316 and 337 nm denoted by B_1 and B_2, respectively, superimposed on the short-wavelength-side shoulder of the intense A_1 band as shown in figure 2(a).

Excitation spectra are obtained by monitoring the intensities of the luminescence at fixed wavelengths. The excitation spectrum of the A_1 band at 360 nm in CNYF consists of an intense band around 315 nm and the satellite bands on the shorter-wavelength side as shown in figure 2(b). The peak of the intense band is shifted to longer wavelengths with the increase of the fixed luminescence wavelength and saturated above 400 nm. The excitation spectrum of the B_1 band at 320 nm in figure 2(b) is similar to that of the A_1 band at 360 nm except for the slight shift of the peak to shorter wavelengths.

The features of the luminescence and excitation spectra are very similar to those for LYF [4, 5] and CaF_2 [12], where Ce^{3+} is eightfold coordinated in these crystals, except that their peaks are continuously shifted to long wavelengths. These results lead us to deduce that there are two distinct Ce^{3+} centres with different configurations, corresponding to the (A_1, A_2) and (B_1, B_2) luminescence bands, and that the optical bands (A_1, A_2) are inhomogeneously broadened. The inhomogeneous broadening of the luminescence and excitation bands can be explained in terms of substitutional disorder in CNYF as discussed in relation to Ce^{3+}:$CaYAlO_4$ (CYA) [13, 14].

The excitation bands of the very weak luminescence at 290 and 300 nm in figure 2(b) are coincident with the intense absorption bands with the peaks at 210 and 260 nm in figure 1. Although the absorption coefficients at 210 and 260 nm are fairly large, the 290–300 nm luminescence band is observed only with a high gain. The 210 nm and 260 nm absorption (excitation) bands are very similar to those observed for CaF_2 heavily doped with 0.5 at.% Ce^{3+} [15]. The absorption centres were assigned as corresponding to Ce^{3+} ions in clusters because the absorption coefficient increased as the concentration of Ce^{3+} increased [15]. As the present crystal included about 1.3 at.% Ce^{3+} in the melt, there is a possibility that these bands could be assigned as corresponding to the Ce^{3+} clusters. The luminescence at 290–300 nm is probably quenched by non-radiative energy transfer between clusters and/or between clusters and isolated Ce^{3+} ions or to other centres in the crystal.

Figure 3 shows a typical decay curve of the Ce^{3+} luminescence intensity at 370 nm with excitation of 315 nm in CNYF measured at 300 K. The curve is fitted to a single exponential. The lifetime of 41 ns is very close to that (40 ns) in LYF [5] and that (40 ns) in CaF_2 [12].

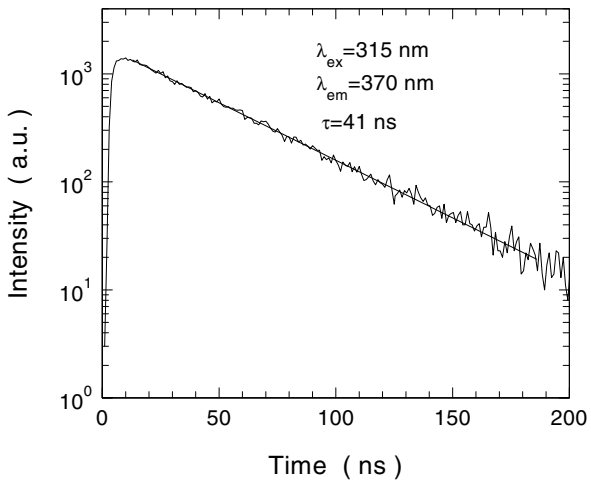

Figure 3. The decay curve of the Ce^{3+} luminescence intensity at 370 nm with 315 nm excitation in $CaNaYF_6$, measured at 300 K. The solid curve showing a single exponential with a lifetime of 41 ns fits the observed data.

Figure 4(a) shows the lifetime and peak intensity ($t \sim 0$) as functions of fixed wavelengths of the Ce^{3+} luminescence in CNYF measured with the 315 nm excitation at 300 and 77 K. The lifetime in each curve increases with increasing luminescence wavelength. The lifetimes below 350 nm and above 450 nm have large experimental errors because of the weak luminescence intensities. Their curves at 300 and 77 K are almost the same within experimental errors. The peak-intensity spectra are coincident with the Ce^{3+} luminescence spectra obtained by the cw UV excitation in figure 2(a). In addition, the decay curves of the Ce^{3+} luminescence were measured with a different excitation wavelength of 260 nm at 300 and 77 K (not shown). These curves were almost the same as those with the 315 nm excitation within

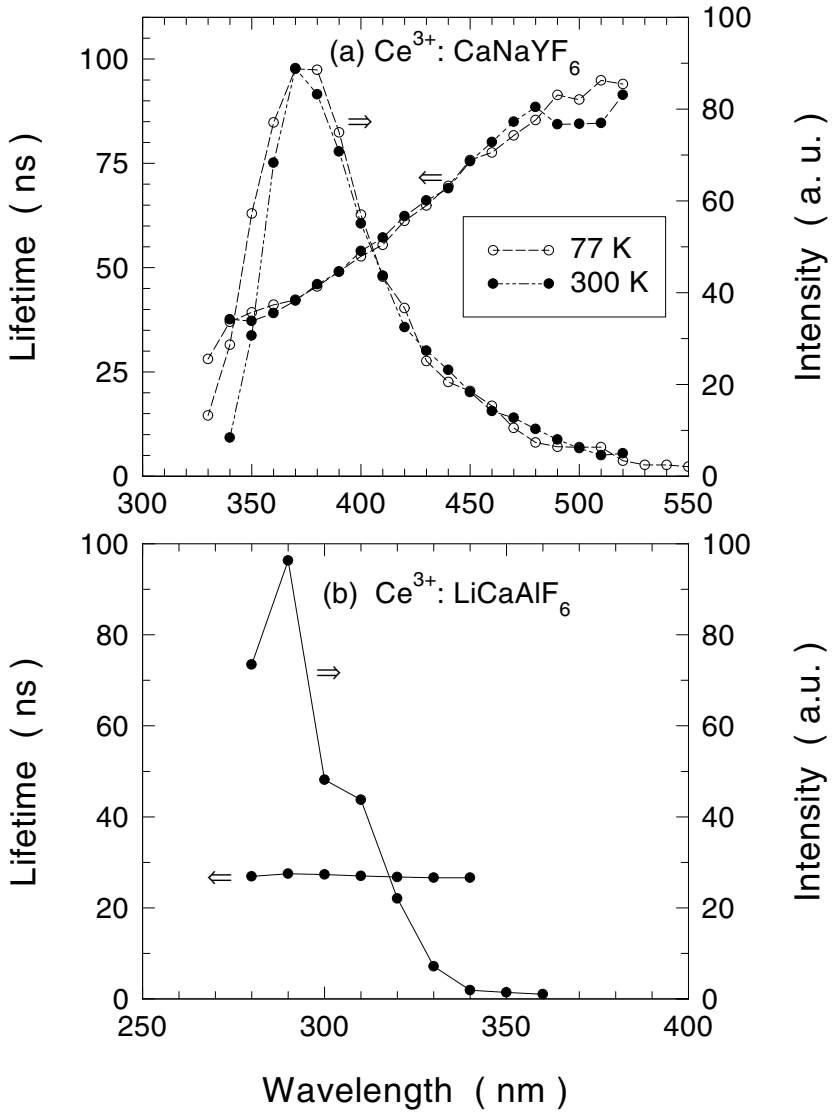

Figure 4. The lifetime and peak intensity ($t \sim 0$) of the Ce^{3+} luminescence as functions of the wavelength at 77 and 300 K for (a) $CaNaYF_6$ in comparison with those measured at 300 K for (b) $LiCaAlF_6$.

experimental errors. The peak intensities for the luminescence at 290–300 nm were not enhanced at 77 K; that is, the non-radiative decay rates were not suppressed through decreasing temperature. In consequence, the non-radiative decay may be due to concentration quenching, being independent of temperature.

The approximately linear dependence of the lifetime on the luminescence wavelength is due to substitutional disorder produced by the random occupation of Ca^{2+}, Na^{+}, and Y^{3+} at the common cation sites in the CNYF crystal. Comparing an ordered system with the disordered system, the lifetime and initial intensity of the Ce^{3+} luminescence in LiCAF measured with excitation of 270 nm at 300 K are shown in figure 4(b). The lifetime of 28 ns is in agreement with that (28 ns) reported in reference [6] and independent of the luminescence wavelength. In consequence, the fairly broad Ce^{3+} luminescence and the variation of the lifetime in CNYF are strongly associated with inhomogeneous broadening of the luminescence, while the Ce^{3+} luminescence in LiCAF corresponds to homogeneous broadening.

4. Discussion

4.1. Numerical deconvolution of the luminescence and excitation spectra

Complexes consisting of a central Ce^{3+} ion and eight F^{-} ligand ions at cubic corners show cubic symmetry. The ^2D excited state of Ce^{3+} splits into the E_g and T_{2g} orbital states in O_h cubic symmetry, the lowest excited state being E_g. The degenerate E_g state is further split into two non-degenerate states by a non-cubic component—for example, distortions produced by the random occupation of the second-nearest-neighbour $Na^{+}/Ca^{2+}/Y^{3+}$ ions in CNYF. The magnitude of the non-cubic component is larger; the energy splitting between the lower E_g excited-state levels is larger. The large crystal-field splitting reduces the energy separation between the lowest excited and ground states, resulting in a red-shift of the Ce^{3+} luminescence band. This expectation is in agreement with the experimental results observed for the Ce^{3+}:CNYF crystal.

Next, we discuss inhomogeneous broadening of the Ce^{3+} luminescence in CNYF, which occurs through the transitions from the lowest excited state to the $^2F_{5/2}$ and $^2F_{7/2}$ ground states of Ce^{3+}. The luminescence spectrum is assumed to be represented by the sum of two Gaussian bands:

$$I(\epsilon) = \sum_{i=1}^{2} I_i \exp\left(-\frac{(\epsilon - \epsilon_i)^2}{2\Gamma_i^2}\right) \tag{1}$$

where ϵ_i and Γ_i are the peak energy and width of the ith band where subscripts $i = 1$ and 2 denote the transitions to the $^2F_{5/2}$ and $^2F_{7/2}$ ground states, respectively.

A comparison of the observed luminescence spectra in CNYF with curves calculated using equation (1) is shown in figure 5(a). The calculated curves (dashed lines) fit the observed spectra (solid lines) with different excitation energies of 37 000, 31 300, and 29 400 cm^{-1}. The spectrum excited at 37 000 cm^{-1} is decomposed into four Gaussians. This implies the existence of two different Ce^{3+} centres corresponding to the (A_1, A_2) and (B_1, B_2) bands in figure 2(a). The spectra excited at 31 300 and 29 400 cm^{-1} are decomposed into two Gaussians. The intensity of the A_2 bands relative to that of the A_1 bands increases with the decrease of the excitation energy, resulting in an enlargement of the linewidth of the total luminescence spectrum. The peak positions ϵ_i and widths Γ_i of the (A_1, A_2) and (B_1, B_2) bands with three different excitation energies are summarized in table 1. The energy difference (2100–2600 cm^{-1}) between ϵ_1 and ϵ_2 for each centre is approximately equal to the energy separation ($\sim$ 2200 cm^{-1}) of $^2F_{5/2}$ and $^2F_{7/2}$.

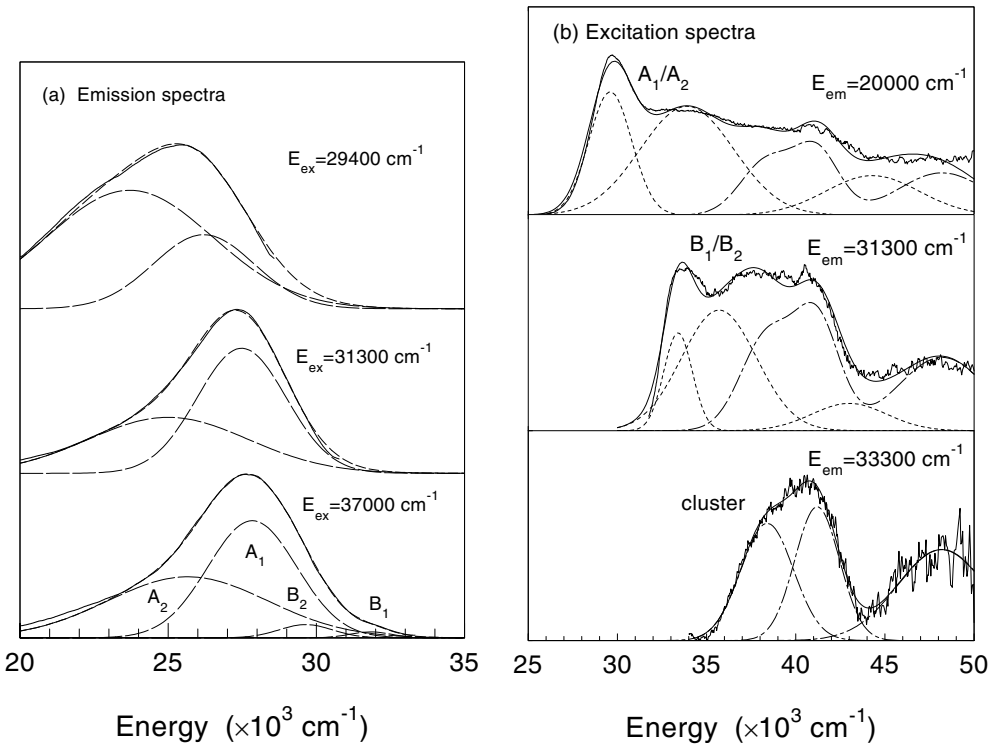

Figure 5. The decompositions of (a) the Ce^{3+} luminescence spectra with different excitation energies and (b) the excitation spectra with different luminescence energies into Gaussians for $CaNaYF_6$. The calculated components of the Gaussians are represented by dashed, dotted, and dotted–dashed lines. The dotted–dashed curves in (b) are calculated to fit the observed excitation spectra with the assumption that the 33 300 cm^{-1} excitation components are included in the excitation spectra.

Table 1. The parameters of the decomposed line shape of the Ce^{3+} luminescence in $CaNaYF_6$.

Excitation energy (cm^{-1})	Band	Peak energy (cm^{-1})	Width (cm^{-1})
37000	A_1	27800	1500
	A_2	25700	2700
	B_1	31800	700
	B_2	29600	900
31300	A_1	27500	1500
	A_2	24900	2700
29400	A_1	26200	1700
	A_2	23700	2800

The width of the B_1 band in CNYF is roughly half of that of the A_1 band. The relatively narrow bands (B_1, B_2) in CNYF may be assigned as corresponding to Ce^{3+} centres occupied in somewhat ordered configurations in CNYF [9, 10, 13, 14]. The line shape of the luminescence spectrum is close to that of Ce^{3+} at the ordinary Ca^{2+} sites in LiCAF [6, 7] except for the peak positions.

Next, we consider the line shapes of the excitation spectra as shown in figure 5(b). The excitation spectrum at $E_{em} = 33\,300$ cm^{-1} (see the spectrum for 300 nm in figure 2(b)) is decomposed into three Gaussians. This spectrum is assigned as corresponding to Ce^{3+} in a cluster as discussed in section 3 [15]. The excitation spectra at $E_{em} = 31\,300$ and $20\,000$ cm^{-1} are decomposed into several Gaussians with the assumption that the excitation spectrum at $E_{em} = 33\,300$ cm^{-1} is superimposed on the dominant Ce^{3+} excitation spectrum and that their relative intensities change as a fitting parameter. The dotted and dotted–dashed curves in figure 5(b) represent the components of the excitation bands from the isolated Ce^{3+} ions and the Ce^{3+} ions in the clusters, respectively. The calculated curves fit the observed excitation spectra very well. The sums of the dotted curves for the excitation spectra at $E_{em} = 31\,300$ and $20\,000$ cm^{-1} represent the intrinsic excitation spectra of the B_1/B_2 and A_1/A_2 luminescence spectra, respectively. The features are very similar except as regards the magnitude of the energy splitting. As the calculation includes the contribution from the clusters, energy transfer from the clusters to the isolated Ce^{3+} ions is expected to occur in CNYF. However, there is another interpretation for the line-shape analyses. The excitation spectrum at $E_{em} = 31\,300$ cm^{-1} would include both contributions from the isolated Ce^{3+} ions and the Ce^{3+} cluster, if their luminescence bands overlap at $\sim$31 300 cm^{-1}. The excitation spectrum at $E_{em} = 20\,000$ cm^{-1} is decomposed into five Gaussians, corresponding to five non-degenerate 5d excited states of the isolated Ce^{3+} ions. In consequence, it is very difficult to conclude from the less structural excitation spectra whether the energy transfer from the cluster to the isolated Ce^{3+} ions occurs in CNYF. We need further experiments to confirm the energy-transfer model.

4.2. Inhomogeneous broadening of the Ce^{3+} luminescence

In order to examine inhomogeneous broadening, the peak energy of the decomposed luminescence band as a function of the excitation energy is plotted in figure 6. The peak energy is increased gradually with the increase of the excitation energy, saturated around $31\,000$ cm^{-1} and nearly constant above $32\,000$ cm^{-1}. The energy regions below and above $\sim$32 000 cm^{-1} correspond to the optical transitions from the $^2F_{5/2}$ ground state to the lowest and higher excited states, respectively. Electrons excited to the higher excited energy levels relax to the lowest excited energy levels of various Ce^{3+} complexes in the crystal through non-radiative multi-phonon processes. The following luminescence includes the contribution from the various Ce^{3+} complexes. Then, the peak energy is almost independent of the excitation energy. On the other hand, electrons excited directly in the lowest excited energy level relax to the zero-phonon vibronic level in the same lowest excited state and de-excite radiatively to the ground state. As monochromatic light can excite selectively Ce^{3+} complexes according to a distribution of the disordered configurations, the peak of the luminescence band is shifted to lower energy with decreasing excitation energy.

The linear dependence of the peak energy of the Ce^{3+} luminescence on the excitation energy for CNYF is the same as has been observed for CYA [13]. This result suggests fairly large inhomogeneous broadening of the Ce^{3+} luminescence as a consequence of the random distribution of $Ca^{2+}/Na^{+}/Y^{3+}$ in different unit cells in CNYF. According to the convolution method developed for Cr^{3+}:glasses [16], the line shape of the luminescence spectrum of Ce^{3+} in CNYF is calculated to be a convolution of the line-shape functions of the intrinsic absorption and luminescence spectra with the distribution function of the energy level, E_{ex}, of the lowest excited state. Here, the distribution function and intrinsic spectrum are assumed to be Gaussians with widths γ and Γ, respectively. The calculated line shape of the luminescence spectrum is

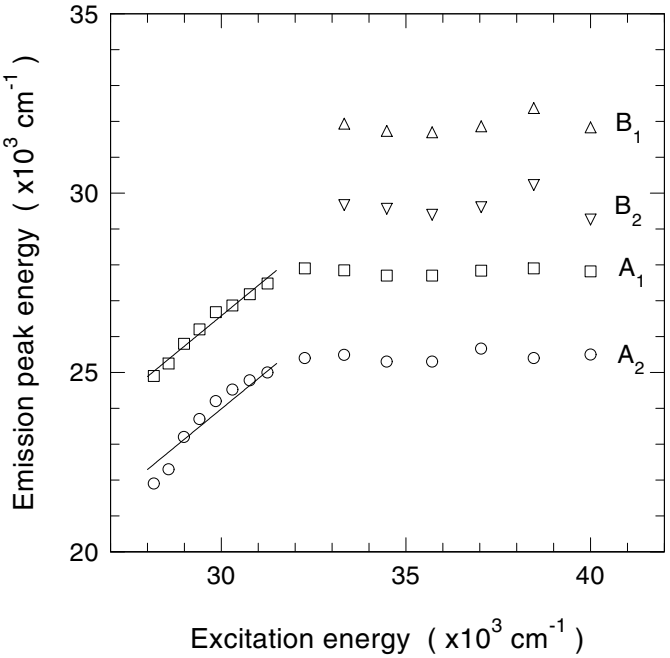

Figure 6. The peak energies of the decomposed luminescence bands as a function of the excitation energy for $CaNaYF_6$. The straight lines for the A_1 and A_2 bands are calculated by the least-squares method. The slope is 0.85.

represented by a Gaussian with a peak energy and width

$$\epsilon^i_- = \frac{E^i_0\Gamma^2 + E_{ex}\gamma^2}{\Gamma^2 + \gamma^2} - 2S\hbar\omega \tag{2}$$

$$\Gamma_{em} = \sqrt{\Gamma^2 + \gamma'^2} \tag{3}$$

where γ'^2 $(=\Gamma^2\gamma^2/(\Gamma^2 + \gamma^2))$ is an inhomogeneous width of the luminescence and E^i_0 $(i = 1, 2)$ is the energy with maximum probability for the distribution function of the energy corresponding to the transition from the lowest excited state to the $^2F_{5/2}$ or $^2F_{7/2}$ ground state [16]. ϵ^i_- and Γ_{em} are coincident with the parameters ϵ_i and Γ_i of the decomposed luminescence bands in table 1.

The slopes of ϵ^i_- versus E_{ex}, being equal to $\gamma^2/(\Gamma^2+\gamma^2)$, are 0.85 for the A_1 and A_2 bands in CNYF. The ratio of γ^2 to Γ^2 is $\simeq$5.7, resulting in $\gamma/\Gamma \simeq 2.4$ and $\gamma' \simeq 0.92\Gamma$. This result shows that the width (γ) of the energy distribution of the lowest excited state is about double that (Γ) of the intrinsic spectrum and that the inhomogeneous width (γ') of the luminescence is comparable to the homogeneous width (Γ).

4.3. The distribution of the lifetime

The lifetime of the Ce^{3+} luminescence in CNYF changes from 38 to 90 ns when the wavelength increases from 340 to 480 nm. In order to examine this trend, the lifetimes observed in various Ce^{3+}-doped fluoride crystals, $KMgF_3$ [17], BaF_2 [18], $SrAlF_5$ [19], CaF_2 [12], $BaMgF_4$ [20], $LiCaAlF_6$ [6], $LiYF_4$ [5], $BaLiF_3$ [21], and various Ce^{3+}-doped oxide crystals, $CaAlYO_4$ [13], $CaAl_{12}O_{19}$ [22], $Ca_2Al_2SiO_7$ [23], $Lu_3Al_5O_{12}$ [24], $YAlO_3$ [24], $Y_3Al_5O_{12}$

[24, 25], are plotted in figure 7. The horizontal values are the peak wavelengths of the Ce^{3+} luminescence bands. Some crystals have two data: the short lifetime is due to Ce^{3+} occupied at the ordinary sites and the long lifetime is due to Ce^{3+} perturbed by the charge compensator in the crystals. The lifetime (40 ns) of the dominant luminescence component at 360 nm in CNYF is very close to those in CaF_2, $SrAlF_5$, $LiYF_4$, and $BaMgF_4$, where Ce^{3+} is eightfold coordinated. The wavelengths and lifetimes in CNYF increase continuously, obeying the linear relation over wide ranges. The lifetimes of Ce^{3+} with ordered configurations in the normal fluoride crystals decrease from 50 to 20 ns with decreasing wavelength. All data points for the fluoride crystals are close to a straight line in figure 7. Although the variations of the lifetimes and the wavelengths in the oxide crystals are larger than those in the normal fluoride crystals except CNYF, the slope of the lifetime versus the wavelength is slightly smaller than in the fluoride crystals.

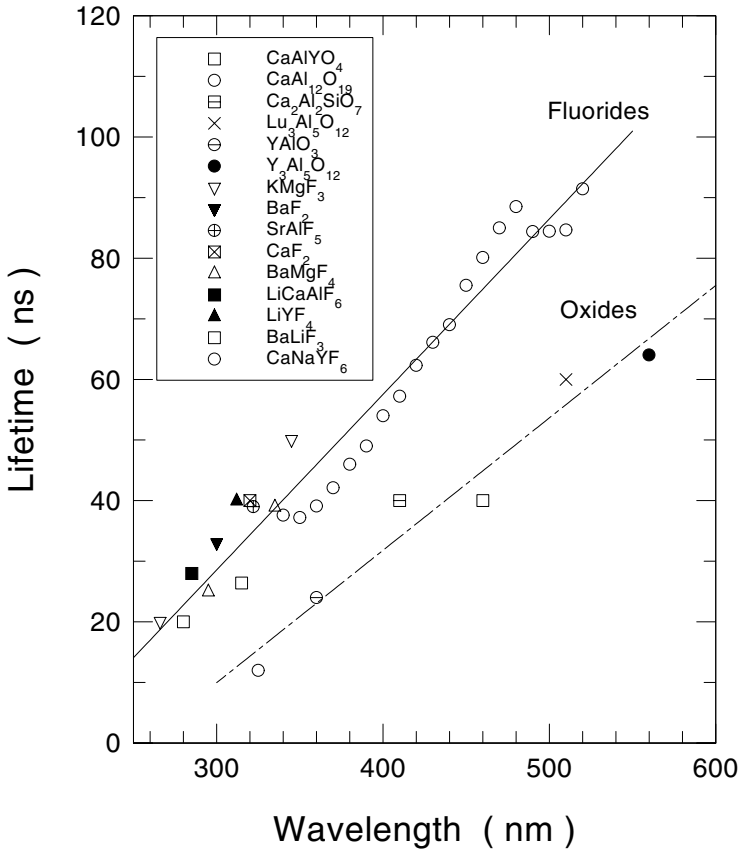

Figure 7. The lifetimes of the Ce^{3+} luminescence in various fluoride and oxide crystals versus the peak wavelength of the luminescence bands including the data for CNYF from figure 4(a). The straight lines are a guide to the eye.

The distribution of the lifetime in CNYF is strongly associated with disordered systems. First, we discuss the energy levels and eigenfunctions of Ce^{3+} with the disordered configurations in CNYF. The disorder is produced by a distribution of cation vacancies or interstitial F^- ions as charge compensators and random substitution of Ca^{2+}, Na^+, and Y^{3+} near to Ce^{3+} ions in CNYF, resulting in variation of the microscopic sizes of the Ce^{3+} cubes and lowering

symmetry of the cubes. The size of the cube is associated with the magnitude of the expansion of the wavefunction of the lowest 5d excited state in the crystal. As the size becomes small resulting in mixing of the wavefunctions of the central Ce^{3+} ion and F^- ligand ions, the centre of gravity of the 5d-excited-state energy levels is reduced [8]. This reduction is regarded as the nephelauxetic effect [3]. Lowering symmetry, which is associated with odd-parity distortions of the cubes, mixes the opposite-parity wavefunctions. For example, the 4f-orbital wavefunction of the ground state mixes with the 5d-orbital wavefunctions of the excited states and the 2s-orbital wavefunctions of the F^- ligand ions. The 5d-orbital wavefunction of the lowest excited state mixes with the p-orbital wavefunctions of the central Ce^{3+} and F^- ligand ions. These mixing coefficients are calculated to be inversely proportional to the energy separation between these states perturbed by the odd-parity distortion. Thus, the effects on the size and symmetry reduce the coefficients of the pure 4f-orbital and 5d-orbital wavefunctions of the ground state and lowest excited state, respectively, and cause the energy shift of the lowest 5d excited state to lower energy. The increase of the Ce^{3+} lifetime in CNYF corresponds to the decrease of the spin-allowed $5d \rightarrow 4f$ electric dipole transition probability—that is, a decrease in the coefficient of the ground state and lowest-excited-state wavefunctions of Ce^{3+}. As the lifetime and wavelength are equal to the inverse of the electric dipole transition probability and the energy separation, respectively, the lifetime is expected to increase linearly when the wavelength increases.

In consequence, the disorder can explain qualitatively why the large inhomogeneous broadening of the Ce^{3+} luminescence in CNYF gives the large distribution of the lifetime. However, it is necessary to explain quantitatively the difference in optical data between the fluoride and oxide crystals as shown in figure 7. Calculation of the energy levels and eigenfunctions of Ce^{3+} ions with various modelling configurations in the crystals using a computer should be done by the same method as has been applied to the system of Ce^{3+}-doped $BaLiF_3$ [26].

5. Conclusions

The random substitution of Ca^{2+}, Na^+, and Y^{3+} at their common lattice sites in CNYF produces a distribution of non-cubic components of distortions of the Ce^{3+} cubes. The magnitude of the non-cubic component determines the energy levels of the 5d excited states and the $^2F_{5/2}$ and $^2F_{7/2}$ ground states and the mixing coefficients of opposite-parity wavefunctions into the ground state and lowest 5d excited state. These effects give inhomogeneous broadening of the Ce^{3+} luminescence and the distribution of the lifetime in the CNYF crystal. In consequence, the luminescence is shifted to near-UV and blue/green regions and the width is fairly substantially broadened. This feature suggests that the CNYF crystal has a potential as a new Ce^{3+}-active material capable of lasing with wider tunability from the near-UV to blue/green regions.

Acknowledgment

One of the authors (M Yamaga) is indebted to Corning for a Research Grant Award.

References

[1] Moulton P 1985 *Laser Handbook* vol 5, ed M Bass and M H Stitch (Amsterdam: North-Holland) p 282
[2] Blasse G and Grabmaier B C 1994 *Luminescent Materials* (Berlin: Springer)
[3] Henderson B and Imbusch F G 1989 *Optical Spectroscopy of Inorganic Solids* (Oxford: Clarendon) ch 5

[4] Ehrlich T D J, Moulton P F and Osgood R M 1978 *Opt. Lett.* **4** 184
[5] Okada F, Togawa S, Ohta K and Koda S 1994 *J. Appl. Phys.* **75** 49
[6] Marshall C D, Speth J A, Payne S A, Krupke W F, Quarles G J, Castillo V and Chai B H T 1994 *J. Opt. Soc. Am.* B **11** 2054
[7] Yamaga M, Lee D, Henderson B, Han T P J, Gallagher H and Yosida T 1998 *J. Phys.: Condens. Matter* **10** 3223
[8] Kodama N, Yamaga M and Henderson B 1998 *J. Appl. Phys.* **84** 5820
[9] Yamaga M, Yosida T, Fukui M, Takeuchi H, Kodama N, Inoue Y, Henderson B, Holliday K and Macfarlane P I 1996 *J. Phys.: Condens. Matter* **8** 10 633
[10] Yamaga M, Macfarlane P I, Henderson B, Holliday K, Takeuchi H, Yosida T and Fukui M 1997 *J. Phys.: Condens. Matter* **9** 569
[11] Hollingsworth G J and McClure D S 1993 *Phys. Rev.* B **48** 13 280
[12] Pogatshnik G J and Hamilton D S 1987 *Phys. Rev.* B **36** 8251
[13] Kodama N, Yamaga M and Henderson B 1996 *J. Phys.: Condens. Matter* **8** 3505
[14] Yamaga M, Kodama N, Yosida T, Henderson B and Kindo K 1997 *J. Phys.: Condens. Matter* **9** 9639
[15] Loh E 1967 *Phys. Rev.* **154** 270
[16] Yamaga M, Henderson B, O'Donnell K P and Gao Y 1991 *Phys. Rev.* B **44** 4853
[17] Francini R, Grassano U M, Landi L, Scacco A, D'Elena M, Nikl M, Cechova N and Zema N 1997 *Phys. Rev.* B **56** 15 109
[18] Wojtowicz A J, Szupryczynski P, Glodo J, Drozdowski W and Wisniewski D 2000 *J. Phys.: Condens. Matter* **12** 4097
[19] Dubinskii M A, Schepler K L, Semashko V V, Abdulsabirov R Yu, Korableva S L and Naumov A K 1998 *J. Mod. Opt.* **45** 221
[20] Yamaga M, Imai T and Kodama N 2000 *J. Lumin.* **87–89** 992
[21] Yamaga M, Imai T, Shimamura K, Fukuda T and Honda M 2000 *J. Phys.: Condens. Matter* **12** 3431
[22] Jeon H S, Kim S K, Kim S C, Park S H, Park H L and Mho S I 1997 *Solid State Commun.* **102** 555
[23] Kodama N, Tanii Y and Yamaga M 2000 *J. Lumin.* **87–89** 1076
[24] Lempicki A, Randles M H, Wisniewski D, Balcerzyk M, Brecher C and Wojtowicz A J 1995 *IEEE Trans. Nucl. Sci.* **42** 280
[25] Weber M J 1973 *Solid State Commun.* **12** 741
[26] Marsman M, Andriessen J and van Eijk C W E 2000 *Phys. Rev.* B **61** 16 477